

Projected Range, Stragglng and Sputtering Yield of the Ion-Impingement of Inert Gases in Group IV, InP and GaAs Semiconductors

J.D. Femi-Oyetero*, O.E. Oyewande

Department of Physics, University of Ibadan, Ibadan, Nigeria

(Received 02 October 2014; published online 25 March 2015)

One of the major challenges in ion implantation and sputtering process (especially in thin film deposition) is to get a shallow or very deep profile and maximum sputtering yield respectively. In this paper, we simulate the projected range, lateral straggle, longitudinal straggle and sputtering yield of inert gas ions (He⁺, Ne⁺, Ar⁺, Kr⁺, Xe⁺, Rn⁺) impinged in group IV elements (C, Si, Ge, Sn, Pb), InP and GaAs against different parameters (ion energy and angle of incident ion), using the TRIM Monte-Carlo Code as embedded in SRIM. In particular, we generated a result on the consistency of the projected range, lateral and longitudinal straggle with the angle of incident ion using ion energies 1 KeV and 10 KeV. However an inconsistency exists in the sputtering yield and we noticed that maximum sputtering yield occurs for certain incident angle. In conclusion, the results presented here provides parameters needed to get low or high projected range and stragglng, and also the exact incident angle needed in getting the maximum sputtering yield for the ion-target combinations used.

Keywords: Impingement, Simulation, Sputtering Yield, TRIM, Stragglng, Semiconductor.

PACS numbers: 61.43.Bn, 61.43.Dq, 61.72.Ww

1. INTRODUCTION

Group IV and III-V semiconductors have found applications in telecommunications and electronics industries, notable examples are optoelectronic devices, laser diodes, LEDs, heterojunction bipolar transistors, amongst others [1-3]. Some of these Group IV and III-V semiconductors are C, Si, Ge, Sn, Pb, InP and GaAs. The band structure of these semiconductors are very similar because they do crystallize in the same crystallographic structure and they also have similar electronic outer orbitals [1, 3]. A lot of effort has been made to improve semiconductors at nanoscale, especially through ion implantation and sputtering process with the use of inert gas ions [17].

Sputtering, being trendy in the scientific community, has created a lot of interest, and this has led to numerous research on molecular dynamics simulation of sputtering, improved transport equations of ions, sputtering for ion thrusters in space science and so on [4-7, 14, 18]. These researches have been applied in various forms; one of the prominent ones is in semiconductor industries, as in etching, thin film deposition, cleaning or polishing of semiconducting materials for better performance.

Over the years ion implantation and sputtering yield data for elemental targets were compiled regularly {Crookes (1891), Anderson & Bay (1891)} [15] till recent [16, 17, 19, 26] because of need for them in applications, and for validation of theoretical approaches so that theory can help minimize costs and effort through its predictions of parameter choices that can yield desired outcomes in experimental investigations. To the best of our knowledge much work has not been reported on the ion-target combinations with the energies used under this study.

In this work, we achieved consistency of the projected range and stragglng, however an inconsistency was seen

in the sputtering yield and a definite angle of incidence of the impinging ion was discovered for maximum sputtering yield. We performed more analysis of the sputtering yield than projected range and stragglng because of its widely known inconsistency.

2. BACKGROUND

2.1 The Ion-Solid Interaction

When an ion bombards a target material, several things can happen. The ones of interest are ion implantation and sputtering (which poses much challenge). The most basic principle is energy and momentum conservation. In any collision, momentum is conserved. If the collision is elastic, kinetic energy is also conserved. When these energetic ion or projectile impinges on a solid surface called the target, it loses energy through a series of binary collisions known as *collision cascades* with the target atoms and finally comes to a rest and at this stage it is referred to as implanted or dopant atoms. The distance traversed during this process is known as the *range*.

Consequently pugnacious collision cascades zones are extended roughly from the surface to the distance of maximum energy deposited into the target. Now target atoms or recoils which have got enough energy from the projectiles to overcome their surface binding energy (SBE) are knocked out from the surface, a phenomenon called *sputtering* and these ejected target atoms are termed as sputtered atoms. Putting the center of mass coordinate frame into consideration, the energy transferred, T , in the collision from the incident projectile to the target particle can be evaluated [20]:

$$T = \beta E_0 \sin^2 \frac{\theta}{2} = \frac{4E_c M_c}{M_2} \sin^2 \frac{\theta}{2} \quad (2.11)$$

* femi.oyetero@yahoo.com

Where

$$\beta = \frac{4M_1M_2}{(M_1 + M_2)^2}, \quad E_c = \frac{E_0M_2}{M_1 + M_2}, \quad M_c = \frac{M_1M_2}{M_1 + M_2}$$

M_1 and M_2 are the mass of the incident particle and target particle, respectively, E_0 is the initial energy of the incident particle, T is the energy transferred to the target atom, and θ is the scattering angle between the particles. The maximum energy transfer T_{\max} occurs during a head-on collision so that:

$$T_{\max} = \beta E_0 \quad (2.12)$$

The final angle of scatter θ , can be expressed in terms of initial center of mass energy, E_c the potential, $V(r)$ and an impact parameter, p is given below (Ziegler et al. 1984), where r_{\min} is the distance of closet approach during the collision [20]:

$$\theta = \int_{r_{\min}}^{\infty} \frac{pdr}{r^2 \sqrt{1 - \frac{V(r)}{E_c} - \frac{p^2}{r^2}}} \quad (2.13)$$

$$r_{\min} = \frac{d}{2} \left(\csc \frac{\theta}{2} \pm 1 \right) \quad (2.14)$$

Where d is the collision diameter.

By taking the initial seed value, $\theta = \pi$ and iteratively integrating over the entire collision path, the final angle of scatter for the projectile (θ) can be evaluated in terms of the initial center of mass energy E_c , the interatomic potential $V(r)$ and the impact parameter, p [20]. Ziegler, Biersack, and Littmark (ZBL) (1984) optimized a function that was originally developed by Lindhard, Scharff and Schiott (LSS) (1963). This result was a generalized analytical expression called the *Universal Screening Function* and this was used to model interatomic potentials given by:

$$V(r) = \frac{Z_1Z_2e^2}{aR} \mathcal{O}(R) \quad (2.15)$$

Where $\mathcal{O}(R)$ is the universal screening function, $R = r/a$ is the reduced interatomic separation, Z_1 and Z_2 are the atomic numbers of the each of the two interacting species, and $V(r)$ is the functional form of the interaction potential between the two atoms.

The stopping power $S(E)$ is the average energy transferred when summed overall impact parameters and is given as:

$$S(E) = \int_0^{\infty} T(E, p) 2\pi p dp = 2\pi\beta E_0 \int_0^{p_{\max}} \sin^2 \frac{\theta}{2} p dp \quad (2.16)$$

Thus, both the conservation of momentum and the interatomic potential are taken into account when the nuclear stopping power of an incident ion in a target material is considered.

2.2 The Sigmund's Theory of Sputtering

A widely accepted quantitative description of the process of ion sputtering was developed by Sigmund

[10]. He derived a set of transport equations describing the energy transfer during the sputtering process. A practically important result of Sigmund's theory is the prediction of the deposited energy distribution: the ion deposited at an arbitrary point inside the bulk of the target material and then spreads its kinetic energy according to the Gaussian distribution:

$$E(r) = \frac{\epsilon}{(2\pi)^{3/2}} \exp\left(\frac{-Z'^2}{2\sigma^2} - \frac{X'^2 + Y'^2}{2\mu^2}\right) \quad (2.21)$$

Where ϵ denotes the total energy carried by the ion. (X', Y', Z'), is the Cartesian coordinate immediately beneath the surface of the target material. σ and μ are the widths of the distribution in directions parallel and perpendicular to the incoming beam respectively, also referred to as lateral and the longitudinal straggle respectively. The mean energy deposition depth due to an ion traveling inside the bulk of the material is given by:

$$a(\epsilon) = \frac{1-m}{2m} \gamma^{m-1} \frac{\epsilon^{2m}}{NC_m} \quad (2.22)$$

Where N is the target atom density, C_m is a constant dependent on the parameters of the interatomic potential and the exponent $m = m(\epsilon)$ varies slowly from $m = 1$ at high energies to $m \approx 0$ at very low energies. In the region of intermediate energies, i.e. for ϵ between 10 and 100KeV, $m \approx 1/2$ and we can approximate the energy deposition depth as, $a = a(\epsilon)$.

If shadowing effects and re-deposition of the eroded material are both ignored, the normal erosion velocity at an arbitrary point in the target material is given by:

$$V_0 = p \int_R dr \phi(r) E(r) \quad (2.23)$$

Where the target material constant, p depends on the surface binding energy (SBE) and scattering cross-section and is given as [7]:

$$P = \frac{3}{4\pi^2} \frac{1}{NU_0C_0} \quad (2.24)$$

Also, Sigmund [10] published an extensive theoretical analysis of sputtering; he derived a comprehensive scheme which led to estimates of sputter yields and their dependence on ion type, energy and angle of incidence. These set of analysis was based on work developed by Lindhard et al, Robinson, Sigmund & Sanders and Thompson [23-25]. He calculated the sputtering yield assuming a random slowing down of particles in an infinite medium [10]. He also developed an integrodifferential equation for yield from the Boltzmann transport equation that is a function of collision cross sections, and atomic binding energies. His formulation of sputtering yield is given as:

$$Y(E) = \frac{0.042}{U_b} \alpha S_n(E) \quad (2.25)$$

The parameter α is a function of the target to ion mass ratio and can be estimated as [29]:

$$\alpha = 0.15 + 0.13 \frac{M_2}{M_1} \quad (2.26)$$

$S_n(E)$, which is the energy dependent nuclear stopping cross section can be calculated with the analytical function developed by Lindhard [10,22] and is given by:

$$s_n(E) = 84.78 \frac{Z_1 Z_2}{(Z_1^{2/3} + Z_2^{2/3})^{1/2}} \left(\frac{M_1}{M_1 + M_2} \right) s_n(\varepsilon) \quad (2.27)$$

Calculating the nuclear stopping cross section requires calculation of the reduced elastic cross section, which is a function of the reduced energy. Thus the reduced energy ε is given by [10]:

$$\varepsilon = \frac{0.03255}{Z_1 Z_2 (Z_1^{2/3} + Z_2^{2/3})^{1/2}} \left(\frac{M_1}{M_1 + M_2} \right) E \quad (2.28)$$

The reduced elastic cross section can be calculated with the analytical expression [27]:

$$s_n(\varepsilon) = \frac{3.441\varepsilon^{1/2} \ln(\varepsilon + 2.718)}{1 + 6.355\varepsilon^{1/2} + \varepsilon(-1.708 + 6.882\varepsilon^{1/2})} \quad (2.29)$$

The Sigmund formula is valid at high ion energy [9, 25]. At these high energies, sputtering processes are as a result of collision cascades, which are modeled by the Sigmund formula. This phenomenon is also known as the High-energy cascade dynamics.

3. METHODS

The TRIM Monte Carlo Code has been employed for the methodology because MC methods allow more rigorous treatment of elastic scattering, and explicit consideration of surfaces and interfaces. Additionally, MC models allow energy and angular distributions to be readily determined. Energy transfer models of this sort are based on the linear superposition of sequential event [28]. In order to analyze the projected range, lateral straggle, longitudinal straggle and the sputtering yield, the simulations were carried out only along 10000 Å target width, for the accommodation of all the ions (1000 in number), during the calculation, at incident angles 0°, 10°, 20°, 40°, 60° and 89.9° ($0^\circ \leq \theta < 90^\circ$) and incident ion energies 1 KeV and 10 KeV. The layer depth is single layered for both single element (e.g. Carbon) and two elements (e.g. GaAs) target materials.

The calculation employed is the detailed calculation with full damage cascades. This option follows every recoiling atom until its energy drops below the lowest displacement energy of any target atom. Hence all collisional damage to the target is analysed. Incident ions and recoils are tracked through their slowing down process until their energy falls below a predetermined energy or they are so far from the surface that they are no longer candidates for sputtering [20].

Target layers with more than one element i.e. GaAs and InP were treated as a single layer with two elements. The target layer densities are the natural density of the element while for InP and GaAs, they are the calculated density value for the compound:

$$\rho_{\text{target material}} = \frac{m_{\text{layer1}} + m_{\text{layer2}}}{V_{\text{layer1}} + V_{\text{layer2}}} \quad (3.11)$$

$$\rho_{\text{InP}} = 4.56095 \text{ g/cm}^3, \rho_{\text{GaAs}} = 5.8155 \text{ g/cm}^3$$

The sputtering yield for GaAs and InP is the total sputtering yield for the compound respectively. The simulation of He⁺-(C, Si, Ge, Sn, Pb, InP, GaAs), Ne⁺-(C, Si, Ge, Sn, Pb, InP, GaAs), Ar⁺-(C, Si, Ge, Sn, Pb, InP, GaAs), Kr⁺-(C, Si, Ge, Sn, Pb, InP, GaAs), Xe⁺-(C, Si, Ge, Sn, Pb, InP, GaAs) and Rn⁺-(C, Si, Ge, Sn, Pb, InP, GaAs) were carried out one after the other, in order to generate values for the projected range, lateral straggle, longitudinal straggle and sputtering yield at incident angles 0°, 10°, 20°, 40°, 60° and 89.9° ($0^\circ \leq \theta < 90^\circ$) for each ion energies 1KeV and 10KeV .

Finally, a sample being, GaAs (10000); where the first elemental layer is Ga and the second elemental layer is As. The target layer (GaAs) was then impinged with Xe⁺ of incident energy 10KeV at an incident angle of 60° (Measured from the axis perpendicular to the target material i.e. x-axis in this context) and the calculated density value, $\rho_{\text{GaAs}} = 5.8155 \text{ g/cm}^3$ was used.

4. RESULTS AND DISCUSSION

After the simulations were carried out, the generated results were thus analysed. For each of the energies 1 KeV and 10 KeV, the projected range and the longitudinal straggle were found to decline with increasing angle of incidence (measured from the axis perpendicular to the target material i.e. x-axis in this context) [Tables 1-5].

Also the lateral straggle was found to rise with increasing angle of incidence [Tables 1-5]. The sputtering yield was discovered not to be consistent as seen in [Tables 1-5]. Generally, for all target materials the highest sputtering yield occurs when the incident angle is 60° [Not 0°, 10°, 20°, 40° or 89.9°] as seen in [Tables 1 and 2] and [Fig. 1, 2].

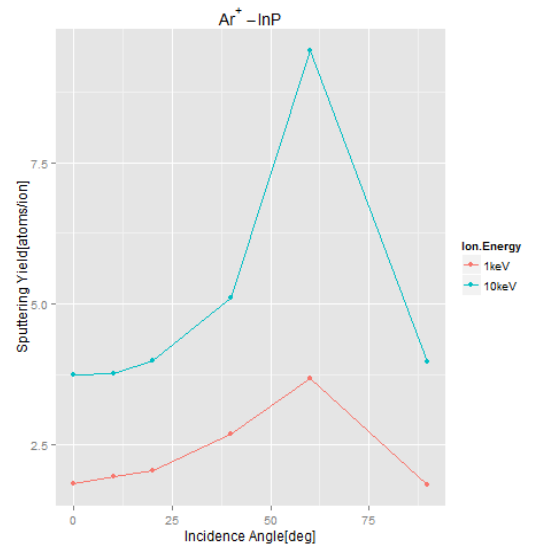


Fig. 1 – Sputtering yield for Ar⁺-InP as a function of incident angle and energy, with maximum sputtering yield occurring at 60° incident angle for both ion energies 1 KeV and 10 KeV

Table 1 – An excerpt showing Ar⁺- (InP and GaAs) at 1 KeV with maximum sputtering yield occurring at 60° incident angle

Ion	Ion Target Material	Angle of Incidence (θ)	Projected Range (Å)	Longitudinal Straggle, μ (Å)	Lateral Straggle, σ (Å)	Sputtering Yield (atoms/ion)
Argon	InP	0	33	19	19	1.8160
Argon	InP	10	32	19	20	1.9340
Argon	InP	20	32	19	22	2.0530
Argon	InP	40	28	17	29	2.6860
Argon	InP	60	25	16	34	3.6850
Argon	InP	89.9	18	12	36	1.8020
Argon	GaAs	0	24	14	15	4.3600
Argon	GaAs	10	24	14	15	4.5570
Argon	GaAs	20	23	14	17	4.7110
Argon	GaAs	40	21	13	21	5.4160
Argon	GaAs	60	17	11	26	7.1140
Argon	GaAs	89.9	13	9	25	3.1240

Table 2 – An excerpt showing Ar⁺- (InP and GaAs) at 10 KeV with maximum sputtering yield occurring at 60° incident angle

Ion	Ion Target Material	Angle of Incidence (θ)	Projected Range (Å)	Longitudinal Straggle, μ (Å)	Lateral Straggle, σ (Å)	Sputtering Yield (atoms/ion)
Argon	InP	0	141	76	80	3.7460
Argon	InP	10	140	78	82	3.7550
Argon	InP	20	136	76	91	4.0040
Argon	InP	40	116	67	121	5.1010
Argon	InP	60	93	61	145	9.4820
Argon	InP	89.9	80	56	164	3.9800
Argon	GaAs	0	103	57	59	7.5440
Argon	GaAs	10	101	56	61	8.1910
Argon	GaAs	20	97	55	69	8.9100
Argon	GaAs	40	85	50	90	11.6330
Argon	GaAs	60	68	45	103	19.7550
Argon	GaAs	89.9	54	40	117	8.4210

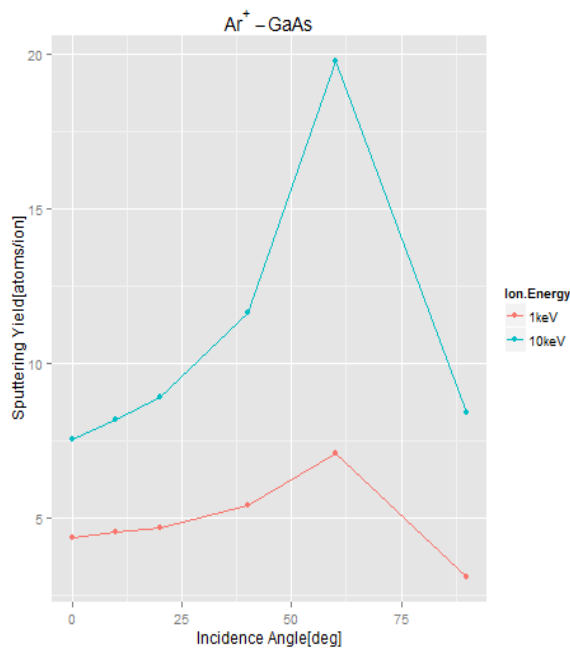


Fig. 2 – Sputtering yield for Ar⁺-GaAs as a function of incident angle and energy, with maximum sputtering yield occurring at 60° incident angle for both ion energies 1 KeV and 10 KeV

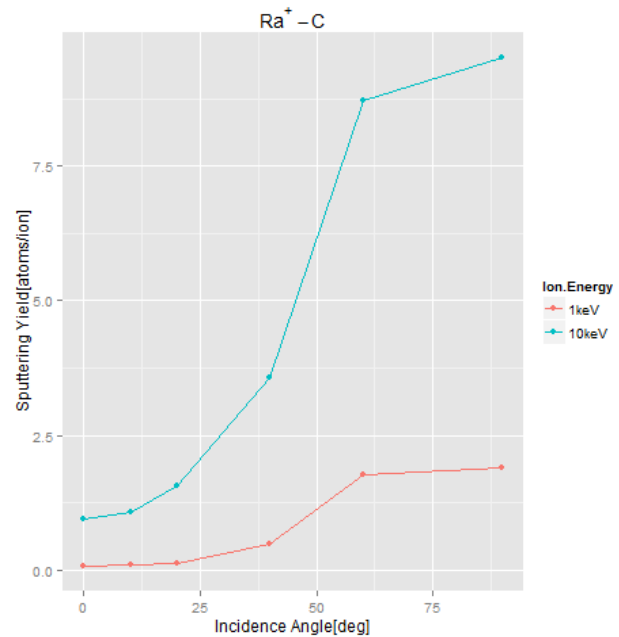


Fig. 3 – Sputtering yield for Ra⁺-C as a function of incident angle and energy, with maximum sputtering yield occurring at 89.9° incident angle for both ion energies 1KeV and 10KeV

Table 3 – Ra⁺-C at 1 KeV with maximum sputtering yield occurring at 89.9° incident angle

Ion	Ion Target Material	Angle of Incidence (θ)	Projected Range (\AA)	Longitudinal Straggle, μ (\AA)	Lateral Straggle, σ (\AA)	Sputtering Yield (atoms/ion)
Radon	Carbon	0	54	4	6	0.0770
Radon	Carbon	10	55	4	11	0.0860
Radon	Carbon	20	53	5	20	0.1320
Radon	Carbon	40	43	5	37	0.4730
Radon	Carbon	60	28	5	50	1.7710
Radon	Carbon	89.9	5	4	58	1.8830

Table 4 – Ra⁺-C at 10 KeV with maximum sputtering yield occurring at 89.9° incident angle

Ion	Ion Target Material	Angle of Incidence (θ)	Projected Range (\AA)	Longitudinal Straggle, μ (\AA)	Lateral Straggle, σ (\AA)	Sputtering Yield (atoms/ion)
Radon	Carbon	0	126	11	15	0.9470
Radon	Carbon	10	125	11	26	1.0800
Radon	Carbon	20	119	12	46	1.5520
Radon	Carbon	40	97	13	83	3.5670
Radon	Carbon	60	64	15	111	8.7210
Radon	Carbon	89.9	15	10	128	9.5130

Table 5 – He⁺- (C, Si, Ge, Sn, Pb, InP and GaAs) at 10 KeV with maximum sputtering yield occurring at 89.9° incident angle

Ion	Ion Target Material	Angle of Incidence (θ)	Projected Range (\AA)	Longitudinal Straggle, μ (\AA)	Lateral Straggle, σ (\AA)	Sputtering Yield (atoms/ion)
Helium	Carbon	0	808	253	282	0.0300
Helium	Carbon	10	789	249	316	0.0160
Helium	Carbon	20	766	247	395	0.0360
Helium	Carbon	40	625	242	582	0.0350
Helium	Carbon	60	448	225	736	0.1090
Helium	Carbon	89.9	278	156	836	0.6400
Helium	Silicon	0	1099	437	553	0.0590
Helium	Silicon	10	1088	453	583	0.0870
Helium	Silicon	20	1040	439	649	0.0370
Helium	Silicon	40	901	425	858	0.0810
Helium	Silicon	60	736	395	1045	0.2050
Helium	Silicon	89.9	524	330	1197	0.7190
Helium	Germanium	0	696	332	452	0.0690
Helium	Germanium	10	703	327	451	0.1160
Helium	Germanium	20	658	320	482	0.0780
Helium	Germanium	40	606	316	581	0.0950
Helium	Germanium	60	549	290	673	0.2880
Helium	Germanium	89.9	484	238	714	0.5690
Helium	Tin	0	652	338	453	0.0980
Helium	Tin	10	620	327	451	0.1540
Helium	Tin	20	637	321	474	0.1150
Helium	Tin	40	593	302	548	0.1410
Helium	Tin	60	531	285	609	0.2800
Helium	Tin	89.9	500	267	657	0.5750
Helium	Lead	0	602	320	453	0.1810
Helium	Lead	10	602	321	448	0.1240
Helium	Lead	20	596	329	447	0.1760
Helium	Lead	40	550	301	526	0.2240
Helium	Lead	60	504	293	555	0.3550
Helium	Lead	89.9	429	247	647	0.5180
Helium	InP	0	900	459	567	0.0980
Helium	InP	10	884	444	596	0.1050
Helium	InP	20	885	436	638	0.0870
Helium	InP	40	764	412	749	0.1010

Helium	InP	60	708	369	889	0.2760
Helium	InP	89.9	593	336	961	0.6830
Helium	GaAs	0	695	346	449	0.1780
Helium	GaAs	10	705	345	475	0.2030
Helium	GaAs	20	670	332	488	0.1750
Helium	GaAs	40	617	317	587	0.3020
Helium	GaAs	60	554	300	691	0.4990
Helium	GaAs	89.9	423	236	773	1.1060

However, exceptions for maximum sputtering yield occur at 89.9° incident angle, for Ra⁺-C at 1 KeV & 10 KeV and He⁺-(C, Si, Ge, Sn, Pb, InP and GaAs) at 10 KeV. The highest sputtering yield for 1 KeV simulations occurs for Xe⁺-GaAs, $\theta = 60^\circ$, with approximate sputtering yield, S.Y = 8 atoms/ion. Also, the highest sputtering yield for 10KeV simulations occurs for Ra⁺-GaAs, $\theta = 60^\circ$ with approximate sputtering yield, S.Y = 32 atoms/ion, making it the highest sputtering yield of all the simulations.

5. CONCLUSION

The observations derived from the results are significant in semiconductor industries. These results

can be used to check for parameters needed to get low or high projected range for ion-target combinations used in this study. Also thin film deposition is widely used for improving the performance of semiconductors, 60° incident angle, produces the highest sputtering yield except Ra⁺-C at 1 KeV & 10 KeV and He⁺-(C, Si, Ge, Sn, Pb, InP and GaAs) at 10KeV which produces highest sputtering yield at 89.9° incident angle. Application of the maximum angle of sputtering yield will help in the improvement of semiconductors with time efficiency in thin film deposition. Finally, experimentalists can also use these results for further research, by paying attention to 60° and 89.9° incident angles for possible maximum sputtering yield under this study.

REFERENCES

1. S. Adachi, *Physical Properties of III-IV Semiconductor compounds: InP, InAs, GaAs, GaP, InGaAs and InGaAsP* (Wiley: 1992).
2. S. T-Ming, *Indium, Phosphide based Integrated Photonic Devices for Telecommunications and Sensing Applications* (PhD Thesis: Massachusetts Institute of Technology, Cambridge, MA: 2012).
3. F. Jerome, *Optical Properties of Semiconductors* (Eidgenossische Technische Hochschule: Zurich: 2008).
4. T.A. Cassidy, R.E. Johnson, *Icarus* **176**, 499 (2005).
5. M.A. Makeev, C. Rodolfo, B. Albert-Laszlo, *Nucl. Instrum. Meth. Phys. Res. B* **197**, 185 (2002).
6. O.E. Oyewande, *Commun. Theor. Phys.* **58**, 165 (2012).
7. R. Cuerno, A.L. Barabasi, *Phys. Rev. Lett.* **74**, 4746 (1995).
8. E.O. Yewande, *Modelling and Simulation of Surface Morphology Driven by Ion Bombardment* (University of Göttingen: Germany: 2006).
9. M.R. Nakles, *Experimental and Modeling Studies of Low-Energy Ion Sputtering for Ion Thrusters*, MS Thesis (Virginia Polytechnic Institute and State University: 2004).
10. P. Sigmund, *Phys. Rev.* **184**, 383 (1969).
11. J.P. Biersack, W. Eckstein, *Appl. Phys. A* **34**, 73 (1984).
12. M.T. Dmonkos, et al., *39th Joint Propulsion Conference* (Huntsville, AL: AIAA 2003-4864: 2003).
13. J.D. Femi-Oyetoro, *On The Ion Distribution, Stragling and Sputtering Yield of the Implantation of Noble Gas Ions in Group IV Elements, InP and GaAs* (University of Ibadan: Nigeria: 2014).
14. P.J. Wilbur, et al., *J. Propulsion Power* **14** No 5, 708 (1998).
15. P. Sigmund, et al., *Symposium on the occasion of the 250th anniversary of the Royal Danish Academy of Sciences and Letters* (Copenhagen: 1992).
16. *Useful Information and Facts about the Practice of Sputtering*. SPECS GmbH Surface Analysis and Computer Technology (Voltastraße 5, 13355 Berlin: Germany).
17. J.P. Green, J. Nemunich, G.E. Thomas, S.L. Schiel, *Noble Gas Sputtering Calculations Using SRIM: ANL/PHY/CP-90696*, CONF-9610183.
18. H. Wilhelm, *NASA CR-13471* (1971).
19. W. Eckstein, et al., *Sputtering Data. Max-Planck-Institut Fur Plasmaphysik*, IPP 9/82, (1993).
20. J.F. Ziegler, J.P. Biersack, M.D. Ziegler, *SRIM-The Stopping and Range of Ions in Matter* (SRIM Co., 285 Cox Neck Rd, Chester, MD, 21619, U.S.A).
21. J.F. Ziegler, J.P. Biersack, *SRIM 2013* (Program and Documentation): <http://www.srim.org>
22. J. Lindhard, V. Nielsen, M. Scharff, P.V. Thomsen, *Mat. Fys. Medd. Dan. Vid Selsk* **33** No 10, 1 (1963).
23. M.T. Robinson, *Philos. Mag.* **12**, 145 (1965).
24. M.T. Robinson, *Philos. Mag.* **12**, 741 (1965).
25. P. Sigmund, *Elements of Sputtering Theory* (Pan Stanford Publishing Pte, Ltd: PSP Review Volume: 2011).
26. J. Geller, N. Veisfeld, *J. Vac. Sci. Technol. A* **6**, 2077 (1988).
27. Y. Yamamura, H. Tawara, *Atomic Data and Nuclear Tables* **62** No 2, 149 (1996).
28. L.A. Giannuzzi, *Introduction to Focused Ion Beams Instrumentation, Theory, Techniques and Practice, XVIII:* (2005): <http://www.springer.com/978-0-387-23116-7>
29. P.K. Ray, V. Shutthanandan, *NASA/CR-1999-209161* (1999).
30. A.L. Barabasi, H.E. Stanley, *Fractal Concepts in Surface Growth* (New York: Press Syndicate of the University of Cambridge: 1995).
31. R.M. Bradley, P.D. Shipman, *Phys. Rev. Lett.* **105**, 145501 (2010).
32. F.C. Motta, P.D. Shipman, R.M. Bradley, *J. Phys. D: Appl. Phys.* **45**, 122001 (2012).
33. J. Munoz-Garcia, R. Cuerno, M. Castro, *Phys. Rev. B* **78**, 205408 (2008).